

IMAGING OF HIERARCHICALLY STRUCTURED MATERIALS

MEHMET SARIKAYA and ILHAN A. AKSAY

Department of Materials Science and Engineering, and
Advanced Materials Technology Center, The Washington Technology Center,
University of Washington, Seattle, WA 98195

ABSTRACT

We describe techniques used to characterize hierarchically structured synthetic and biological materials. These techniques decipher the structures through the dimensional spectrum from the molecular and atomic scales (10^{-10} m) to the macro scales (10^{-3} m) where the overall shape of the material emerges. Techniques used to image surfaces and internal structures can be categorized according to their wavelength and thus spatial resolution as light, x-ray, and electron microscopy. We also discuss newly emerging microscopy techniques that image surfaces at the atomic level without a focusing lens, such as scanning tunneling and atomic force microscopies, with the aid of field ion microscope and scanned probe microscopes. Transmission electron microscopy (TEM), a unique tool for multipurpose imaging, provides structural information through direct imaging, diffraction, and spectroscopic analysis. We illustrate the major TEM techniques used to analyze structural hierarchy with examples of synthetic and biological materials. We also describe light optical microscopy and scanning probe microscopy techniques, which cover the opposite ranges of the dimensional spectrum at the micrometer and subangstrom levels.

1. INTRODUCTION AND BACKGROUND ON HIERARCHICAL STRUCTURES

Hierarchically structured materials display distinct architectural designs at successively varying length scales, with each level of structure a self-forming entity.¹ In this definition, each level of structure is locally diverse, yet interactive through successive levels, thereby generating a larger overreaching structure with unique properties that reflect the contribution of phenomena taking place at various levels of the hierarchy. Although the internal structures in each level of the hierarchy provide the intrinsic properties of material, it is the interfaces between the hierarchical levels that allow interaction between levels and provide continuity at each step throughout the entire structure.

In synthetic materials,^{1,2} such as crystalline ceramics or metals, the hierarchy may include the levels summarized in Figures 1 and 2, with the smallest level a few angstroms containing a single atom. The next scale in the hierarchy would be the unit cell which represents the smallest crystallographic entity. In a single crystalline material, the unit cell would repeat itself through the entire material in three dimensions with no higher level of hierarchy. In the single crystalline state, thermodynamically dictated imperfections such as vacancies, interstitials, and dislocations constitute the first level of structural features in the hierarchical ladder.³ Most materials of technological importance, though, are not single crystalline, but instead are aggregates of finite size single crystalline grains (Figure 1).³ In some cases, these grains may exhibit domain structures. Second phase precipitates within grains are also commonly observed features.² Higher level aggregation of grains can deliberately be introduced when it is essential to design more complex structures.⁴ Figure 3 is a set of transmission electron microscope (TEM) images from a nanoparticle colloidal-gold system in which the different levels of the structure are revealed. The individual particles, their aggregation, the formation of first generation voids, clusters of particles, second and higher generation voids, and cluster of aggregates clearly demonstrate the formation of a structural hierarchy on a wide dimensional scale.⁴

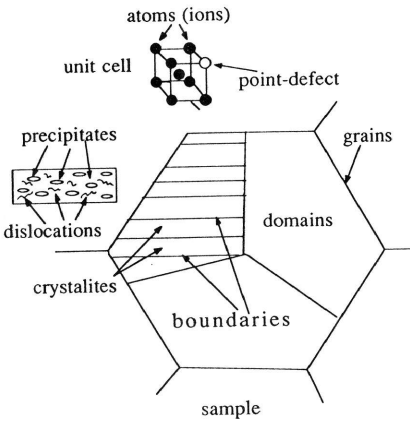


Figure 1. Schematic illustration of hierarchy in synthetic materials.

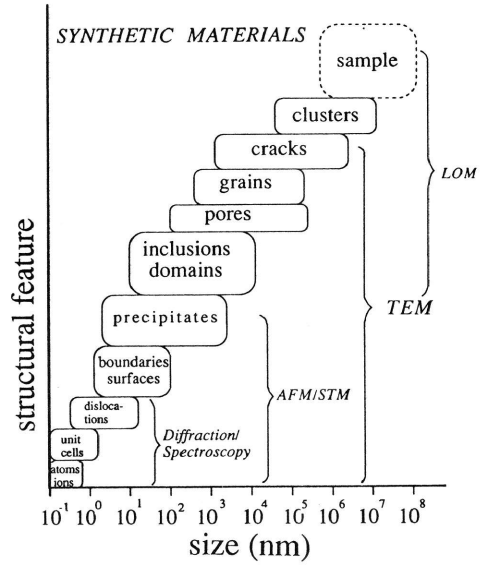


Figure 2. Variation of structural features with respect to size in synthetic materials.

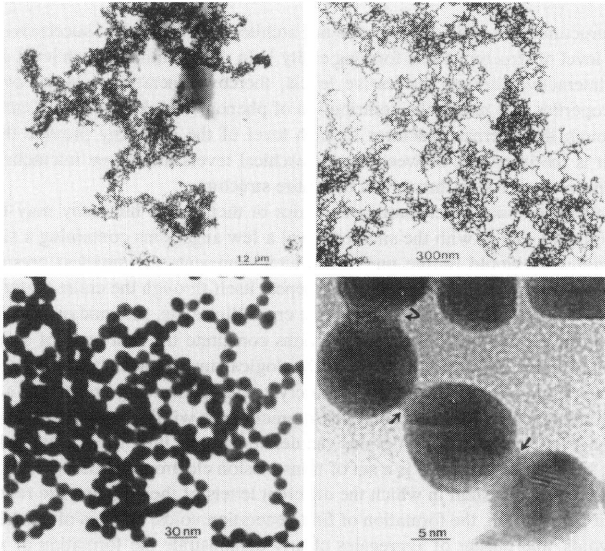


Figure 3. TEM images of colloidal gold particles suspended on a carbon film. At low magnification, only the shape of the cluster is apparent (a); at higher magnifications, smaller pores and the individual particles are revealed (b and c). Lattice and interface structures of particles are resolved at the highest magnification (d) (from Ref. 4(b)).

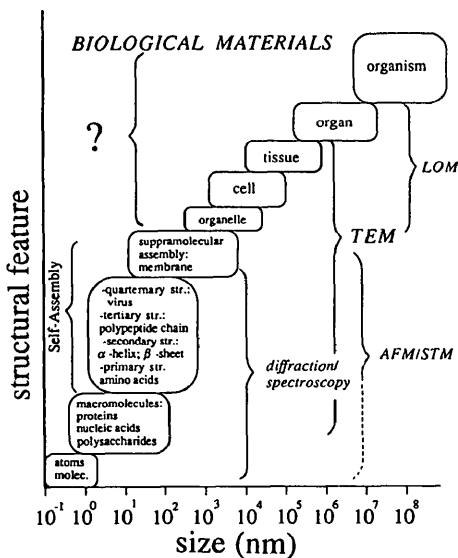


Figure 4. Hierarchical structures in biological materials.

At the tertiary level, long chains of molecules form and, in groups of three, wind in helices to form individual collagen fibrils. Tropocollagen fibrils are triple helices of collagen fibrils a few nanometers thick.⁵ In the next layer up, these fibrils wind together in groups of three or more (similar to the previous level) to form microfibrils (3–4 nm in diameter). Higher levels of structure incorporate subfibril, fibril, fascicles, and finally tendon through the dimensional hierarchy from 10 nm, 100 nm, 50 μ m, and 0.5 mm in diameter, respectively. A similar hierarchy forms in many biological tissues, including hair and skin.⁵

Like soft tissues, biological hard tissues also have a hierarchical structure that starts at the molecular level. But here it is much less defined and is difficult to infer. For example, the hierarchy in bone above the micrometer dimension has been well established,⁷ but at lower levels, the hierarchy in the inorganic component is not yet well established.⁸ Even in this case, however, some new evidence illuminates the nature of the structural units that make up the calcium phosphate component of the tissue.⁹

In an accompanying paper, we discuss the structural hierarchy of nacre, a hard tissue found in mollusks, beginning at the dimension of the nanometer level and extending to the macroscale.¹⁰ The nacre section of the red abalone shell contains CaCO_3 in the form of aragonite platelets organized as "bricks" held together by an organic matrix.^{11–13} At the microscale, the platelets are crystallographically related to each other in that each one is twin-related to the one next to it (first generation twins). Each platelet, furthermore, has three, four, or six domains that are themselves twin-related to each other (second generation twins). The integrity of the structure in a given single crystalline platelet is maintained by the formation of $\{110\}$ twins at the nanometer scale (third generation twins). The crystallographic, morphological, and geometrical configuration of the platelets suggest that they are space filling tiles with multiple twins.¹⁴ We find that the space filling is accomplished by the formation of local spirals, which themselves form spirals that continue up the scale to finally form the shape of the shell.¹⁴

Hierarchy in biological materials is much more organized and well studied.^{5,6} Almost all soft tissues are made up of hierarchical structures that start at the molecular level as organic molecules, usually as molecules formed of C, H, N, O, and sometimes S and P.⁵ Macromolecules in the secondary structures are long-chain organic molecules. At the third level, organic structures are composed of these macromolecules as aggregates in the form of enzymes, which themselves self-assemble into specific shapes forming quaternary structures, such as structural proteins and polysaccharides. Specific functions of the proteins and other macromolecular aggregates are defined by these quaternary structures. At higher levels of hierarchy, the structures of biological soft tissues successively form membranes, organelles, cells, tissues, and organs, as indicated in the chart shown in Figure 4.⁵

In tendon, a classic example of hierarchy in a biological material,⁶ the structure resembles a common engineering fiber composite in which the fibers are uniaxially embedded in a binding matrix. The hierarchy in tendon, however, is much more established and the structure is highly ordered.⁶ The primary and secondary structures are ions and molecules. At

In order to discern the hierarchy in a given synthetic or biological structure, it is essential to use techniques that give structural information at many dimensional levels, from atomic to macro scales. There are many imaging, spectroscopy, scattering, and diffraction techniques that provide structural information.¹⁵ Our objective in this paper is to provide a concise description of imaging techniques that provide the most direct visual investigation of the structures. We limit our discussion only to the length scale from atomic to micron dimensions since it is the architecture of this range that most directly influences the architecture and the properties of larger structures.

2. MICROSCOPIES TO INVESTIGATE HIERARCHY IN MATERIALS STRUCTURES

Two classes of microscopy techniques are used to image hierarchical structures (Table I). The first, surface imaging, uses radiation reflected from the surface of a sample or uses the interaction of a scanning tip with a surface. The technique, therefore, allows imaging of only surfaces or surface layers of materials. With the second class, internal structure imaging, primary radiation passes through, and interacts with the matter and produces an image of the bulk structures, internal interfaces, lattice and microstructural defects, and second phase particles. In the following sections, these microscopy techniques are described in order of their capability to resolve hierarchical structures at increasingly smaller length scales.

Table I. A Summary of Microscopies

Microscopy	Resolution		
	Surface Imaging	Bulk Imaging	Wet
light optical (LOM)	0.5 μm , 50 nm (NFOM)	0.2 μm (CM)	Y
x-ray (XRM)	—	50 nm	Y
electron	5 nm (1 nm) (SEM)	1.5 \AA (HREM)	N
field ion	<1 nm (FIM)	2 nm (atom probe)	N
scanning probe:			
atomic force (AFM)	0.5 nm (lateral), <1 \AA (vertical)	—	Y
tunneling (STM)	1 \AA (lateral), <<1 \AA (vertical)	—	N

2.1 Light Optical Microscopy

Light optical microscopy (LOM) has traditionally been used to image surface structures of biological and physical materials at about the 500 nm resolution level.¹⁶ Figure 5 is an LOM image of a low carbon/low alloy steel showing the hierarchical structure in a synthetic material.¹⁷ The microstructure displays a single pre-austenite grain (original phase) containing domains, or packets, of martensite (product phase) that are rotated with respect to each other at 70° or 110°, i.e., four {111} variants of an austenite (face-centered cubic) crystal.¹⁸ Each packet is actually composed of lath-shaped martensite crystallites (parallelepiped-shaped crystallites are 0.5 μm thick, 2-5 μm wide, and 5-20 μm long) all in the same crystallographic orientation belonging to the same {111} austenite variant. Therefore, the image in Figure 5 actually shows three levels of hierarchy and compares well with the model described in Figure 1.

The resolution in LOM can be improved to several hundred nanometers in the transmission mode, for example in confocal microscopy (CM). In CM, the image is obtained by scanning a rastered sample with a laser beam focused to a certain depth that allows three-dimensional imaging of the sample with improved resolution since the light scattered from parts other than the portion of the specimen being illuminated is rejected from the optical system.¹⁹ In the newly developed near-field optical microscopy (NFOM) technique, the resolution is not limited by diffraction from the aperture, and, therefore, is not limited by the wavelength of light.²⁰ A focusing lens is not used in this technique; instead the light wave

is confined to a pipe with an exit aperture radius less than the wavelength of radiation used.²¹ The sample is placed at the near field, i.e., at a distance less than the diameter of the aperture. The size of the

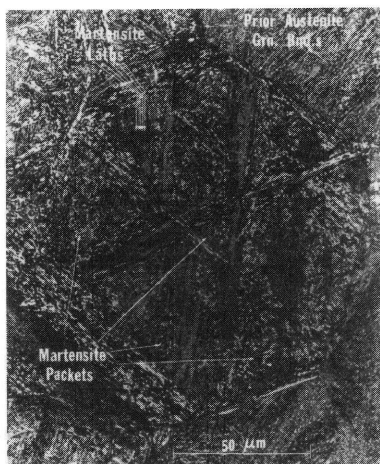


Figure 5. LOM image reveals hierarchy in the structure of a low-alloy steel (from Ref. 17).

probe that illuminates the sample is a geometrical projection of the aperture and not its Fourier transform, unlike the far-field case, and, thus, diffraction from the aperture is not allowed, so Abbe's diffraction limited resolution limitation does not apply. High spatial frequencies of the sample can be imaged, limited only by the size of the illuminating (imaging) aperture and by the material of which it is made (opacity). This pushes the limits of resolution in light optical imaging to 50 nm as demonstrated experimentally, and theoretically to levels less than 10 nm.²⁰

2.2 X-ray Microscopy

It is possible to increase resolution in the image beyond that provided by visible LOM using shorter wavelengths of x-rays. X-rays are also preferable to electrons because of their usefulness in studying biological materials in their natural states under wet or gaseous atmospheres. Because x-rays can neither be reflected nor refracted, focusing them is very difficult; magnified imaging, in the past, has been impossible. Recently, however, x-rays have been successfully focused using Fresnel zone plates to obtain magnified images at resolutions down to 500 Å in imaging or scanning x-ray microscopes.²¹ The zone plates are analogous to glass lenses in LOM and magnetic lenses in EM. To reduce radiation damage, soft x-rays (a 20-40 Å wavelength) are used and the sample is scanned with an x-ray probe,²¹ building the image one picture element at a time, which significantly reduces exposure of the sample to the beam, as in the scanning transmission electron microscope.²² The best resolution depends largely upon the finest zone spacing (now about several hundred angstroms) but is still limited to diffraction aberration from the rings.²³

2.3 Electron Microscopy

Electron microscopy imaging techniques can be divided into three major areas according to their specific image forming means. These three areas are described below with examples.

2.3.1 Scanning and Scanning Transmission Electron Microscopy

In scanning electron microscopy (SEM), a small electron probe formed by a convergent lens is scanned over the surface of a sample by the use of scan coils. The interaction of the incoming electrons with the sample produces secondary electrons from the surface layers that are then collected by a solid-state detector (Figure 6).²⁴ In SEM, the smaller the area scanned, the higher the magnification of the final image. In all scanning microscopy systems, the resolution depends on the effective size of the probe, i.e., the original size of the probe modified by the aberrations of the probe-forming lenses and the modifications that arise from sample-probe interactions. In terms of resolution, electrons at high voltages (20-30 kV) have wavelengths in the subangstrom range (fraction of an angstrom) and hence provide much better resolution than what can be achieved with LOM. Resolution in SEM, roughly defined by

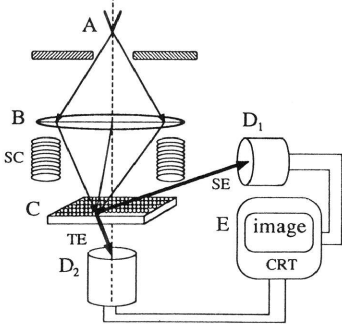


Figure 6. Simplified schematic of the electron microscope. A: electron source, B: objective lens, SC: scan coils, C: sample, TE: transmitted electrons, SE: secondary electrons, D1 and D2: detectors, and E: imaging system. The configuration ABCD1 corresponds to SEM and ABCD2 to scanning transmission electron microscopy (STEM) (the latter also to TEM if the illumination is parallel).

the size of the electron probe, can now be at the nanometer level, and the smallest point detectable on the surface of a sample typically falls between 50 and 100 Å. Smaller electron probes can be achieved in systems with a high-flux electron source (e.g., a field emission gun system) or a probe-forming lens with a low spherical aberration; resolution in the subnanometer range is not difficult to achieve.²⁵

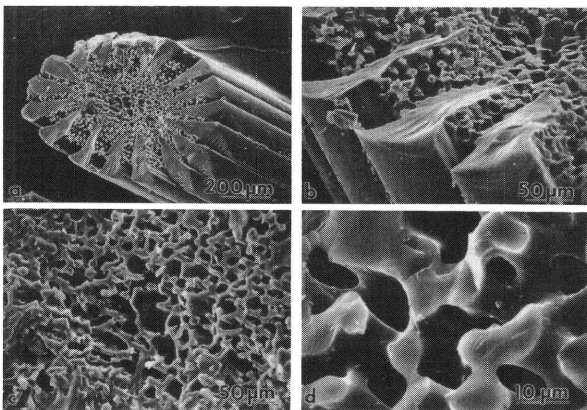


Figure 7. SEM images from fractured sea urchin spine reveal structural detail at different magnifications.

The primary benefit of SEM in imaging surfaces is its large depth of field, which allows examination of rough sample surfaces with large disparities. In LOM, by contrast, only optically polished surfaces can be focused and studied. The value of depth of field is illustrated in Figure 7, where a cross-sectional view of the fractured surface of a sea urchin spine is analyzed. Sea urchin spine is thought to be a single crystalline calcitic (rhombohedral CaCO_3) structure, and yet it has an elaborate microarchitecture. A general view of the fractured surface is seen in Figure 7(a), which illustrates a central hard and "spongy" structure surrounded by the 18 wedge-shaped columns radiating from the center. Both these columns and the spongy structure are seen in detail in Figure 7(c). Finally, in Figure 7(d), a higher magnification image shows the details of the fractured surface of calcite in the spongy portion of the sample, revealing a concoidal fracture.

In the scanning transmission electron microscopy (STEM) mode,²² imaging is accomplished by scanning a small electron probe formed by a strong condenser lens over a sample, just as in SEM. In STEM, however, the sample is thin enough for electron transparency, so images are formed with detectors placed at appropriate positions along the optic axis. In the dark field (DF) mode, STEM can image a single heavy atom or cluster of atoms suspended on a thin amorphous film.²⁶ Atomic resolution images can be achieved with annular DF imaging, obtained using a sufficiently small ($\sim 2 \text{ \AA}$ in diameter) and highly coherent electron probe. This technique has been demonstrated to display atomic number contrast, and hence the ability to distinguish compositional fluctuations at high resolution due to the differences in the scattering powers of different atomic species constituting the sample.²⁶

2.3.2 Transmission Electron Microscopy

The transmission electron microscope is a multipurpose instrument that permits investigation of synthetic and biological samples in three modes of analysis: (i) imaging, (ii) diffraction, and (iii) spectroscopy.²⁷ The fundamental principle of TEM is the same as that of LOM. The primary electrons reach a thin sample in the parallel illumination mode, travel through the sample and are diffracted. A

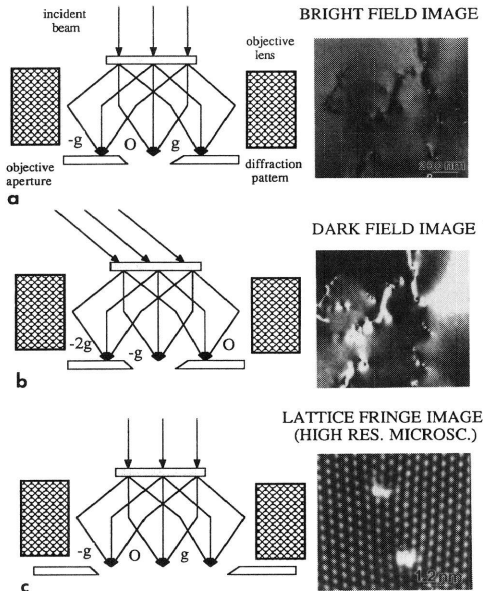


Figure 8. Schematic of formation of TEM bright field (BF) (a), dark field (DF) (b), and high-resolution electron microscopy (HREM) (c) images with corresponding experimental images (from Ref. 28).

magnetic lens (called objective lens, analogous to the glass objective lens in the LOM) focuses the scattered electrons to form the diffraction pattern and the image. In the imaging mode, conventional TEM (CTEM) limits the formation of the image to only one of the diffracted beams. The detail in a CTEM image is produced by many contrast mechanisms arising from amplitude variations in a single electron wave,²⁸ which are introduced because of the interaction of the incoming wave with the sample. The elastically scattered transmitted and diffracted beams are used for bright field (BF) and dark field (DF), respectively. CTEM techniques are used in many imaging studies in synthetic materials and biological tissues to investigate morphology and distribution of the constituent phases at an image resolution of about several nanometers. Figures 8(a and b) show BF and DF images where dislocations are revealed in the matrix of Al.²⁸

In the case of high-resolution TEM (HREM), imaging is performed using many beams, including the central beam (Figure 8(c)).²⁹ The image formed at the back focal plane of the objective lens is an interference pattern, which under ideal circumstances (i.e., small spherical aberration of the objective lens and its defocus) may represent the projected potential of an ultrathin (<10 nm) crystalline sample in the particular orientation in which it is observed.³⁰ Therefore, HREM provides direct imaging of crystalline structures to investigate their atomic configurations at the site of defects, such as dislocations, interfaces, and boundaries³¹ and their long-range ordered structures.³² For instance, Figure 8(c) shows an image of a low-angle boundary in a biogenic aragonitic CaCO_3 crystal where dots represent atomic columns in the structure in the reverse contrast. Edge dislocations at the boundary and the bending of atomic planes near the core of the dislocations are clearly visible.²⁸

In the diffraction mode, diffraction patterns form at the back focal plane of the objective lens through either parallel illumination or convergent illumination of the sample by the beam.²⁷ In the former case, a spot pattern forms, which is generally used to identify crystallographic zone axes and lattice parameters of an examined crystalline sample. The sampled area that gives rise to the diffraction pattern is selected by a field limiting aperture and can be as small as 0.5 μm in diameter. With convergent beam electron diffraction (CBED), the sampled area can be as small as the electron probe (in modern microscopes, less than 1 nm), making the CBED technique the highest spatial resolution diffraction technique available.

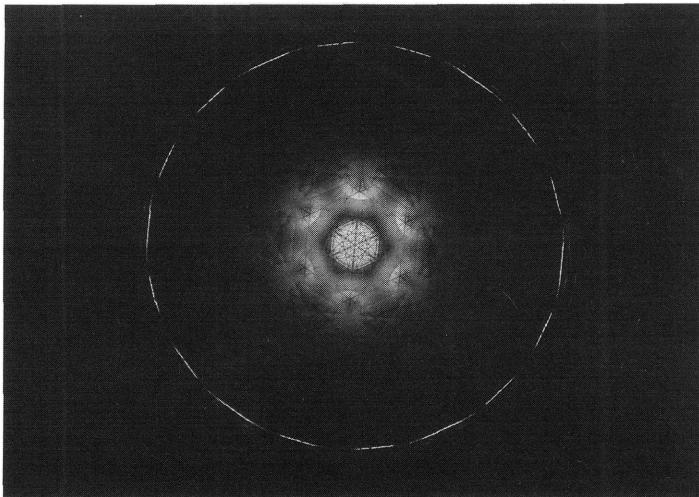


Figure 9. CBED pattern recorded in [001] zone axis orientation from β -SiC (hexagonal) shows details of crystallographic features and symmetries in the zero and higher order Laue zone layers (courtesy of G. H. Kim).

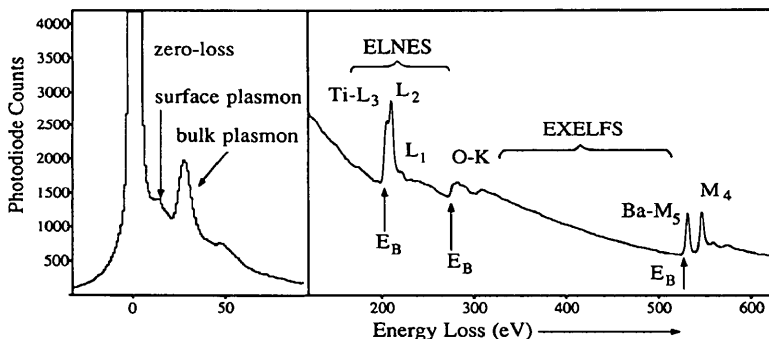


Figure 10. A characteristic EEL spectrum illustrates various regions used for spectroscopic analysis from a sample of BaTiO₃ (spectrum was taken with a parallel detection system at 200 kV).

Due to the finite convergence of the beam, diffracted beams in this case form disks instead of spots, the centers of which are located at the Bragg positions.³³ Because of the interaction of the upper Laue layers, diffraction lines form in the central and diffracted beams (Figure 9). The position of these so-called high-order Laue zone (HOLZ) lines or their absence provides information about the constituent atoms in the unit cell, the unit cell geometry and its lattice parameters, symmetry groups (point and space groups),^{34,35} and internal stresses; CBED, therefore, can be used for analysis of crystalline structures at varying length scales.³³

Spectroscopy, the third mode of operation of TEM, includes energy dispersive x-ray spectroscopy (EDS) and electron energy loss spectroscopy (EELS).³⁶ When an incoming electron probe strikes a TEM sample, it produces x-rays with specific energies characteristic of the constituent elements in the sample. Quantification of these x-rays can provide compositional analysis of the sample from areas defined by the probe diameter, areas as small as a few nanometers.³⁷ Low energy x-rays may be trapped at the window of the x-ray detectors and, thus, limit the compositional analysis to elements with atomic number $Z > 10$, i.e., Na and up.

Electrons passing through the sample will lose some of their initial energy through beam-sample interaction, including the process of x-ray production.³⁸ In EELS, these electrons are examined with respect to their loss in energy, as plotted in Figure 10. The sharp peak at the "zero" position corresponds to those electrons that did not lose any of their energy and corresponds to the zero-loss peak. The low-loss energy region, up to 50 eV, corresponds to the plasmon excitation, including surface and bulk plasmon. From the positions of these peaks, plasmon energies or frequencies can be determined, allowing the estimation of, for example, complex dielectric function. At high losses, edges appear due to inner shell excitations, whose threshold values correspond to the binding energies of the electrons of the K, L, etc., shells (K-edges, L_{2,3} edges). In addition, the shape of the near-edge structure represents the density of states for the empty orbitals and therefore the oxidation state of the element (i.e., near-edge fine structure analysis, ELNES).³⁹ Beyond about 50 eV from the threshold, fine structure in the tail of an edge gives variations similar those found in soft x-ray absorption edges.⁴⁰ This means that the information from the fine structure can be used to deduce near-neighbor interactions and short-range order (e.g., coordination number) that are similar to extended x-ray fine structure (EXAFS).⁴⁰ Such an analysis in EELS is called extended energy loss fine structure analysis (EXELFS).⁴¹ In the sense of providing bonding and electronic information of the structure with or without long-range order (i.e., crystalline or amorphous samples) the EELS technique permits hierarchical structural analysis at the lower end of the structural spectrum.

2.4 Field Ion Microscopy

The formation of an image in the field ion microscope (FIM) is based on the tunneling principle and does not require an image-forming lens.⁴² When an imaging gas, He, for example, is ionized (at 10^{-3} torr) near a positively charged, cryogenically cooled tip of a specimen at a certain voltage, ions are accelerated radially onto a channel plate/fluorescent screen assembly to form an image, which is the magnified projection of the tip. The mechanism by which the imaging gas is ionized is known as field ionization and is based on the electron tunneling process.⁴² At the atomic protrusions on the tip, local field strength is raised, which preferentially ionizes atoms at these positions, and corresponding bright spots form the image. The visible image formed on the screen is a projection of the sample tip and roughly resembles the stereographic projection of the crystalline sample in the direction of the specimen axis.⁴³ The magnification (M) on the screen is determined by the ratio of the distance between the tip and the screen (L) to the radius of the tip (R); for example, for $R = 5$ nm and $L = 5$ cm, then $M = 10^6$. When the tip radius is less than 500 \AA and the tip is kept at the temperature of liquid He, the atomic structure of a conductive sample becomes resolvable. An FIM image consists of an array of bright spots, each of which corresponds to an atom; the atoms are lined at the periphery of concentric terraces centered around crystallographic axes that make up the tip surface. When the temperature of the tip is low ($<10\text{K}$) and imaging gas atoms of small diameter are used (e.g., He), then resolution as small as 2 \AA can be achieved.⁴⁴

2.5 Scanning Probe Microscopy

The scanning probe microscopy system (SPM) uses a probe tip, held by a piezoelectric cantilever, scanned above the sample.⁴⁵ Either the tunneling current between a conductive sample and the tip (in the case of scanning tunneling microscopy (STM))⁴⁵ or the deflection of the cantilever caused by the forces acting between the sample and the tip as it scans above the sample (in the case of atomic force microscopy (AFM)),⁴⁶ is measured as a function of the distance traveled by the probe in the x and y directions. Measurement of the current or the deflection is sufficiently accurate to resolve atomic or molecular corrugations on the surface of the sample and allow topographical analysis of the sample at the atomic resolution. The interaction (in terms of tunneling current or atomic force) between the probe tip and the sample varies exponentially with distance between the sample and the very extreme point on the

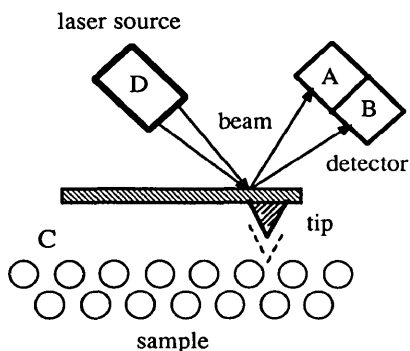


Figure 11. Schematic of an AFM system (in STM, sample is conductive and there is a current tunneling between the tip and the sample).

probe tip; in the STM, for example, the atom at the extreme point of the probe tip allows the tunneling current to pass through. Spatial confinement of the tunneling current into a small cross section allows this technique to image the electron cloud on the surface of the sample in the form of contours around each atom. The resolution in the image, which is only a surface or subsurface image, is defined both vertically and laterally on the plane of the sample. Under favorable experimental conditions, lateral resolution is less than the diameter of the atoms on the surface and easily reaches a fraction of an angstrom. The STM technique has been successfully applied to conductive samples, such as metals and semiconductors but, despite great effort, has not yet successfully imaged biological macromolecules and tissues.^{45,47}

In AFM, the interaction forces between the tip material and the sample thin film or substrate can be measured. These forces, attractive or repulsive, may be as small as a few nanonewtons, and the sample may or may not be an electrical conductor.^{46,48} The sample can thus be imaged in its natural state, biological samples, for example, in an aqueous environment. In the case of repulsive forces, the tip actually touches the surface and can trace over the atoms without damaging the surface of the sample. In AFM, unlike STM, the sample moves with respect to a fixed force sensor containing the tip. The deflection of the cantilever, hence the force between the tip and the sample, can be measured by the aid of a laser beam that is reflected to a detector (Figure 11). Like STM, under favorable conditions (flat crystalline surfaces of graphite, mica, or CaCO_3 , for example) AFM images with atomic corrugations can be produced. Atomic resolution images of more complex surfaces, however, including biological membranes or protein complexes such as DNA, have not yet been reproducibly imaged.⁴⁸

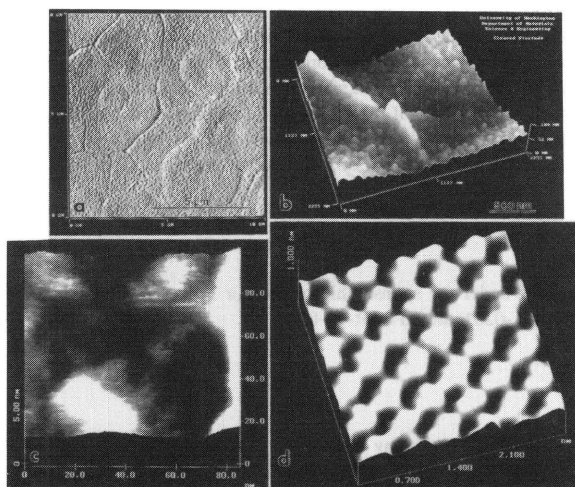


Figure 12. AFM images (a to c) show details of the structure on the cleaved surface of the nacre of a red abalone recorded in water. (d) AFM image of calcite reveals atomic packing on the basal plane (courtesy of Kevin Kjolar, Digital Instruments).

In summary, the usefulness of AFM is threefold: (i) no limitation on samples, (ii) imaging under various environmental conditions, and (iii) a wide range of magnification. The example given in Figure 12 illustrates this point with images recorded in water from the cleaved surface of the nacre of red abalone at increasingly higher magnifications. In Figure 12(a), a scan over the surface covering an area $10 \mu\text{m} \times 10 \mu\text{m}$ reveals multi-edged CaCO_3 (aragonite) platelets in a face-on configuration separated by

grooves of organic matrix. In Figure 12(b), a scan of $2\ \mu\text{m} \times 2\ \mu\text{m}$ reveals that the organic matrix that separates each layer of platelets and over which the cleavage took place is still attached to the surface. Note that the surface is rough and decorated with semispherical beads of organic matrix probably due to deformation during cleavage. In the image, however, the interfaces between the platelets are clearly seen, significantly more deformed than the organic matrix in the interior of the platelets. At higher magnification, or in a smaller scan of $80\ \text{nm} \times 80\ \text{nm}$, the details on the surfaces of the organic beads can be seen in Figure 12(c). Although there is regular image variation on the organic surface, which may be due to the original conformation of the proteins in the organic matrix, the image is not detailed enough to confirm any kind of regular structure. Finally, in Figure 12(d) the atomic resolution in the image of synthetic CaCO_3 (calcite) is sufficient to clearly reveal the lattice of the rhombohedral structure on the basal plane.

3. CONCLUSIONS

Many scattering, spectroscopy, and imaging techniques can provide valuable information, but no single technique is capable of providing all the hierarchical structural information from the atomic to the macro scale. Among the structural characterization techniques, however, the information gathered by TEM may be the most comprehensive. The TEM instrument can simultaneously provide information at all modes of analysis including imaging, diffraction, and spectroscopy, all from the same region with spatial resolutions at the subnanometer and atomic levels. A combination of techniques from the TEM can provide information about the atomic species (CBED, EELS, STEM, HREM); atomic bonding and oxidation states (ELNES); unit cell and its dimensions (HREM, CBED); short-range order (EXELFS); long-range order (CBED and HREM); and defect and morphological analysis (CTEM). TEM, therefore, can truly provide hierarchical information from organic and inorganic samples. TEM, however, is not without limitations, the major ones being that since it is a high vacuum technique, samples in the "wet" state cannot be observed, and because of highly energetic primary electrons, radiation damage can be a problem (especially for biological and amorphous materials). So it is clear that for a comprehensive analysis of structures of materials an arsenal of techniques is required, from light, x-ray, and electron to scanning probe microscopies.

ACKNOWLEDGEMENTS

This work was performed under the sponsorship of the Air Force Office of Scientific Research under Grant Numbers AFOSR-91-0281 and AFOSR-91-0040.

REFERENCES

1. C. S. Smith, "Structural Hierarchy in Science, Art, and History," in *Aesthetics in Science*, J. Wechsler (ed.) (MIT Press, Cambridge, Massachusetts, 1978), pp. 9-53.
2. *Phase Transformations*, edited by H. I. Aaronson and C. M. Wayman (American Society of Metals, Metals Park, Ohio, 1982).
3. F. A. Kroger, *The Chemistry of Imperfect Crystals*, Vol. 2 (North-Holland, Amsterdam, 1974).
4. (a) I. A. Aksay, "Molecular and Colloidal Engineering of Ceramics," *Ceramics International*, **17** [5] 267-74 (1991); (b) M. Sarikaya, "Atomic Resolution Microscopies in Materials," in *Advanced Characterization techniques in Ceramics, Ceramic Transactions*, Vol. 5 (American Ceramic Society, Westerville, Ohio, 1990), pp. 247-86.

5. C. K. Mathews and K. E. van Holde, *Biochemistry* (Benjamin/Cummins Publ., Redwood City, California, 1990).
6. E. Baer, J. J. Cassidy, and A. Hiltner, "Hierarchical Structure of Collagen and Its Relationship to the Physical Properties of Tendon," Chapter 9 in *Collagen: Biochemistry and Biomechanics*, Vol. II, edited by M. E. Nimi (CRC Press, Boca Raton, Florida, 1988), pp. 177-99.
7. M. J. Glimcher, "On the Form and Function of Bone; from Molecules to Organs," *The Chemistry and Function of Mineralized Tissues*, edited by A. Veis (Elsevier, Amsterdam, 1981), pp. 617-73.
8. S. Weiner and W. Traub, "Mineralized Tendon, Bone, and Dentin," *Connect. Tissue. Res.*, **27** [2-3] 86 (1992).
9. H. A. Lowenstam and S. Weiner, *On Biomineralization* (Oxford University Press, New York, 1989).
10. J. Liu, M. Sarikaya, and I. A. Aksay, "A Hierarchically Structured Model Composite: A TEM Study of the Hard Tissue of Red Abalone," this volume.
11. J. D. Currey, "Biological Composites," *J. Mater. Edu.*, **9** [1-2] 118-296 (1987).
12. A. P. Jackson, J. F. V. Vincent, and R. M. Turner, "The Mechanical Design of Nacre," *Proc. Roy. Soc., London*, **B234**, 415-40 (1988).
13. M. Sarikaya and I. A. Aksay, "Nacre of Abalone Shell: A Natural Multifunctional Nanolaminated Ceramic-Polymer Composite Material," Chapter 1 in *Structure, Cellular Synthesis, and Assembly of Biopolymers*, edited by S. Case (Springer-Verlag, New York, 1992).
14. J. Liu, M. Sarikaya, and I. A. Aksay, unpublished work.
15. J. P. Sibilía, *Materials Characterization and Chemical Analysis* (VCH, New York, 1988).
16. R. Hooke, *Micrographia* (Royal Society, London, 1665).
17. M. Sarikaya, Ph.D. Thesis (University of California, Berkeley, LBL Rep. # 15211, 1982).
18. (a) M. Sarikaya and G. Thomas, "Lath Martensites in Low Carbon Steels," *J. Phys.*, Colloque (4) supp. 12, Tome 43, C4-563-68 (1982); (b) M. Sarikaya, H. Togushige, and G. Thomas, "Lath Martensite and Bainite in Low Alloy Steels," in *Proc. of Intl. Conf. on Martensitic Transformations* (Japan Institute of Metals, Tokyo, 1986), pp. 613-18.
19. *The Handbook of Biological Confocal Microscopy*, edited by J. Pawley (IMR, Madison, Wisconsin, 1989).
20. M. Isaacson, "Resolution in Near-Field Optical Microscopy," in *Resolution in the Microscope, Ultramicroscopy*, special issue, edited by M. Sarikaya, in press (1992).
21. M. Howels, J. Kirz, and D. Sayre, "X-ray Microscopes," *Sci. Amer.*, **264** [2] 88-94 (1991).

22. A. V. Crewe, J. P. Langmore, and M. Isaacson, "Resolution and Contrast in the Scanning Transmission Electron Microscope," Chapter 4 in *Physical Aspects of Electron Microscopy and Microbeam Analysis*, edited by B. M. Siegel and D. K. Beaman (Wiley, New York, 1975), pp. 47-62.
23. C. Jacobsen, J. Kirz, and S. Williams, "Resolution in X-ray Microscopes," in *Resolution in the Microscope, Ultramicroscopy*, special issue, edited by M. Sarikaya, in press (1992).
24. *Practical Scanning Electron Microscopy: Electron and Ion Microanalysis*, J. I. Goldstein and edited by H. Yakowitz (Plenum, New York, 1975).
25. D. C. Joy and J. Pawley, "Resolution in the SEM," in *Resolution in the Microscope, Ultramicroscopy*, special issue, edited by M. Sarikaya, in press (1992).
26. S. J. Pennycook, "Z-Contrast STEM for Materials Science," *Ultramicroscopy*, **30**, 58-69 (1989).
27. L. Reimer, *Transmission Electron Microscopy* (Springer-Verlag, Berlin, 1984).
28. M. Sarikaya and J. M. Howe, "Resolution in CTEM," in *Resolution in the Microscope, Ultramicroscopy*, special issue, edited by M. Sarikaya, in press (1992).
29. J. C. H. Spence, *Experimental High Resolution Electron Microscopy* (Oxford University Press, Oxford, 1986).
30. M. A. O'Keefe, "Resolution in High Resolution Electron Microscopy," in *Resolution in the Microscope, Ultramicroscopy*, special issue, edited by M. Sarikaya, in press (1992).
31. O. L. Krivanek, "High Resolution Imaging of Grain Boundaries and Interfaces," *Chemica Scripta*, **14**, 213-20 (1979).
32. J. M. Cowley and D. J. Smith, "High Resolution Transmission Electron Microscopy," *Acta Cryst.*, **A 43**, 739-48 (1989).
33. J. W. Steeds, "Convergent Beam Electron Diffraction," in *Introduction to Analytical Electron Microscopy*, edited by J. J. Hren, J. I. Goldstein, and D. C. Joy (Plenum, New York, 1979), pp. 387-422.
34. M. Tanaka, R. Sito, and H. Sekii, "Point Group Determination by Convergent Beam Electron Diffraction," *Acta Cryst.*, **A39**, 357-68 (1983).
35. J. W. Steeds and R. Vincent, "Use of High Symmetry Zone Axis in Electron Diffraction in Determining Crystal Point and Space Groups," *J. App. Cryst.*, **16**, 317-24 (1983).
36. J. I. Goldstein, "Principles of Thin Film Microanalysis," Chapter 3, pp. 83-120, and N. Zaluzec, "Quantitative X-ray Microanalysis: Instrumental Considerations and Applications to Materials Science," Chapter 4, pp. 121-68, in *Introduction to Analytical Electron Microscopy*, edited by J. J. Hren, J. I. Goldstein, and D. C. Joy (Plenum, New York, 1979).
37. D. B. Williams et al., "Resolution in Energy Dispersive X-ray Spectroscopy," in *Resolution in the Microscope, Ultramicroscopy*, edited by special issue, M. Sarikaya, in press (1992).

38. R. F. Egerton, *Electron Energy Loss Spectroscopy in the Electron Microscope* (Plenum, New York, 1986).
39. R. Brydson, "Interpretation of Near Edge Structure in the Electron Energy Loss Spectrum," *EMSA Bulletin*, 21 [2] 57-67 (1991).
40. E. A. Stern and S. M. Heald, "Basic Principles and Applications of EXAFS," Chapter 10 in *Handbook on Synchrotron Radiation*, Vol. 1, edited by E. E. Koch (North-Holland, Amsterdam, 1983).
41. S. Csiszlag, D. A. Johnson, and E. A. Stern, "Extended Energy Loss Fine Structure Studies in the Electron Microscope," in *EXAFS Spectroscopy: Techniques and Applications*, edited by F. K. Teo and D. C. Joy (Plenum, New York, 1981), pp. 241-54.
42. R. H. Good and E. W. Muller, "Field Emission," in *Handbuch der Physik*, Vol. 21 (Springer-Verlag, Berlin, 1956), pp. 176-231.
43. M. K. Miller and G. D. W. Smith, *Atom Probe Microanalysis: Principles and Applications to Materials Research* (Materials Research Society, Pittsburgh, Pennsylvania, 1989).
44. C. R. M. Grovenor et al., "Ultrahigh-Resolution Chemical Analysis by Field-Ion Microscopy, Atom Probe, and Position Sensitive Atom Probe Techniques," in *Resolution in the Microscope, Ultramicroscopy*, special issue, edited by M. Sarikaya, in press (1992).
45. G. Binnig and H. Rohrer, "Scanning Tunneling Microscopy," *Helv. Phys. Acta*, 55, 726-35 (1992).
46. G. Binnig, C. Quate, and C. Gerber, "Atomic Force Microscope," *Phys. Rev. Lett.*, 56, 930-32 (1986).
47. J. A. Glovchenko, "The Tunneling Microscope: A New Look at the Atomic World," *Science*, 232, 48-53 (1986).
48. P. K. Hansma, V. B. Ellings, O. Marti, and C. E. Bracker, "Scanning Tunneling Microscopy and Atomic Tunneling Microscopy: Applications to Biology and Technology," *Science*, 242, 209-16 (1988).